Ultrafast Buildup Dynamics of Terahertz Pulse Generation in Mode-Locked Quantum Cascade Lasers

Feihu Wang,[1,2,3,4,*] Xiaoqiong Qi,[5] Valentino Pistore,[1] Lianhe Li,[6] Gary Agnew,[5] Edmund Linfield,[6] Giles Davies,[6] Jérôme Tignon,[1] Juliette Mangeney,[1] Aleksandar D. Rakić,[5] and Sukhdeep S. Dhillon[1,†]

[1] *Laboratoire de Physique de l'Ecole Normale Supérieure, ENS, Université PSL, CNRS, Sorbonne Université, Université de Paris, Paris, France*

[2] *Shenzhen Institute for Quantum Science and Engineering, Southern University of Science and Technology, Shenzhen 518055, China*

[3] *International Quantum Academy, Shenzhen 518048, China*

[4] *Guangdong Provincial Key Laboratory of Quantum Science and Engineering, Southern University of Science and Technology, Shenzhen 518055, China*

[5] *School of Information Technology and Electrical Engineering, The University of Queensland, Brisbane QLD 4072, Australia*

[6] *School of Electronic and Electrical Engineering, University of Leeds, Woodhouse Lane, Leeds, United Kingdom*

(Received 27 November 2021; revised 17 September 2022; accepted 7 November 2022; published 19 December 2022)

Ultrashort terahertz pulse generation is essential for a range of proven terahertz applications, from time-resolved spectroscopy of fundamental excitations to nondestructive testing and imaging. Recently, it has been shown that semiconductor-based terahertz quantum cascade lasers (QCLs) can be used to generate pulses as short as a few picoseconds through active mode locking. However, further progress for subpicosecond and high peak power pulse generation is hampered by poor knowledge on how the electric field actually forms in these lasers. Here, we theoretically and experimentally show the amplitude- and phase-resolved buildup of pulse generation through active mode locking, from initiation of pulse generation to the nanosecond steady state. The experimental results, using an ultrafast coherent seeding technique to probe the laser from femtosecond to nanosecond time scales, are in full agreement with the theoretical calculations based on a theoretical model using multimode reduced rate equations. In particular, we show that the electric field buildup to achieve short pulse operation is extremely fast, requiring only a few photon round trips, owing to the ultrafast gain dynamics of the lasers. Further, this shows a gain recovery time of the order of a few picoseconds, an order of magnitude smaller than the photon round-trip time, highlighting that terahertz QCLs are categorically class-*A* lasers. This demonstration marks an important formulism for future progress towards exploring the ultrafast pulse generation buildup dynamics of these complex semiconductor lasers.

DOI: 10.1103/PhysRevApplied.18.064054

I. INTRODUCTION

Mode-locked lasers for ultrashort light pulse generation is an underpinning technology throughout the electromagnetic spectrum, enabling the study of fundamental ultrafast light-matter interactions, and impacting domains stretching from attosecond science to frequency combs. Recently, the domain has been strongly impacted by the advent of time-resolved ultrafast techniques, where laser dynamics can be experimentally investigated on ultrafast timescales [1,2]. This has permitted detailed insights into complex laser buildup behavior, enabling understanding of the fundamental mechanisms of pulse generation and impacting their performance for a broad range of applications.

Ultrashort pulse generation has also been transformed by the advent of mode-locked semiconductor lasers, offering compact and cost-effective systems [3]. This is of particular relevance to the underdeveloped terahertz range [4] where quantum cascade lasers (QCLs) [5] have recently demonstrated ultrashort pulse generation [6–8]. (In contrast, there is a large and important body of work on frequency-modulated QCL frequency combs [9–13]). These QCLs could potentially replace costly and complex optical femtosecond-laser-based terahertz systems [14,15] for key applications stretching from gas metrology to nondestructive testing [4]. Despite these advances,

*wangfh@sustech.edu.cn
†sukhdeep.dhillon@phy.ens.fr

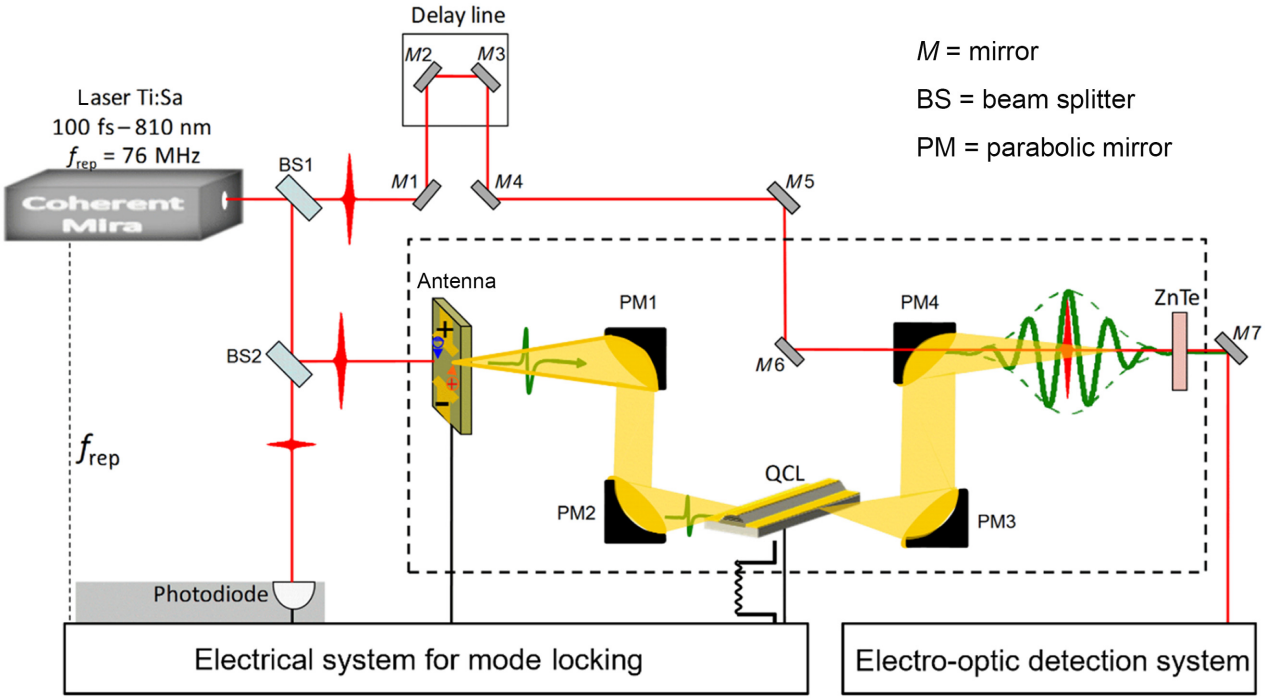

FIG. 1. Experimental setup for the mode-locking buildup dynamics study. Red pulse (line) shows femtosecond optical pulse (path). Green pulses represent terahertz waves. Yellow zones denote terahertz wave path. Black line shows electrical connections.

the understanding of the full-field-resolved dynamics of pulse generation buildup—how the amplitude and phase of mode-locked emission develops from initiation to the steady state—has not been directly demonstrated. In this work, we couple phase-resolved measurements of the emission properties of a QCL with a theoretical model based on multimode reduced rate equations (MM RREs) [16–18] combined with the master equation [19–21], permitting direct observation and simulation of the turn-on field-resolved dynamics of the laser when modulated at the round-trip frequency. In particular, we take advantage of recent advances in ultrafast techniques in the terahertz range, where a phase-resolved single-cycle pulse is used to completely resolve, on femtosecond time scales, the amplitude and phase carried by the radiated electromagnetic field of a terahertz laser [22,23]. This theoretical approach permits a predictive model of ultrashort pulse generation and shows that these lasers' unique ultrafast dynamics permit the electric field buildup to achieve steady-state (nanosecond time scales) mode-locked operation in only a few photon round trips, in agreement with the experimental results.

QCLs are unipolar quantum devices realized on state-of-the-art semiconductor growth [5]. These devices are one of the only practical semiconductor systems that offer gain in the terahertz range, where the "band-structure-by-design" nature of QCLs allows the emission frequency and bandwidth to be entirely engineered [24]. These laser sources have undergone important developments in performance, including significant increases in output power [25] and considerable rises in operating temperature with operation now routinely available on Peltier coolers [26–30]. Recently, active mode locking and harmonic mode locking of these devices has been achieved [31–33]. Mode-locked pulse trains as short as 4 ps have been demonstrated using a Gires-Tournois interferometer integrated within a QCL [6]. Although the mode-locking mechanism of terahertz QCLs has begun to be investigated with insights into the effect of ultrafast QCL dynamics [34], distinct from classical interband semiconductor lasers, its buildup dynamics have remained less studied. Indeed, unlike most other lasers, QCLs are typically classified as class-*A* lasers where the upper laser state lifetime is shorter than the round-trip time. However, there remain considerable variations in reported gain recovery lifetimes of at least an order of magnitude (approximately 5 to 50 ps) [34–37]. The techniques used in these works were typically based on terahertz pump-probe measurements, which were limited in time resolution, in saturating the gain, or limited to below laser threshold investigations. Recent work has shown gain dynamics of less than about 2 ps [38]. Besides, these methods do not permit and do not allow the full characterization of the mode-locking process, from buildup to the steady-state nanosecond regime.

In this paper, we first investigate the free-running emission (i.e., without active modulation) of this laser and

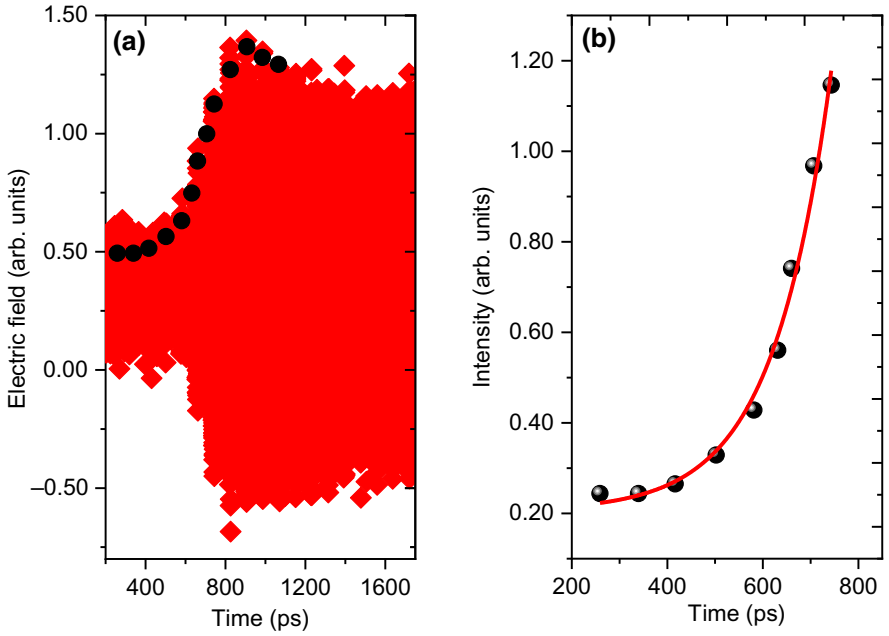

FIG. 2. Free-running switch-on dynamics of the terahertz QCL. (a) Free-running emission of this terahertz QCL from before being switched on to steady state measured using ultrafast time-resolved detection. (b) Black dots denote envelope of the intensity of the cw emission. Red curve denotes exponential fitting of the dynamics range.

analyze its dynamical behavior. Then we actively mode lock the device, which is coupled to an integrated Gires-Tournois interferometer, to generate ultrashort terahertz pulses [6]. From mode-lock initiation until steady-state operation, the full-field emission of this device is completely resolved on femtosecond scales using the proven technique of "injection seeding," where a phase-resolved terahertz pulse and ultrafast gain switching initiates the QCL emission. The experimental setup is presented in Fig. 1. In contrast to the techniques used to investigate mode-locking dynamics of classical solid-state or semiconductor lasers, this ultrafast coherent detection technique resolves inherently the phase and amplitude of the QCL's electric field [37]. Here, the known phase of the input terahertz pulse is used to replace the spontaneous emission of the QCL such that coherent detection of the terahertz emission buildup can be sampled. Thus, the phase-resolved mode-locking buildup dynamics process of lasers can be directly observed in the time domain with femtosecond resolution, which permits the amplitude and phase transients of each frequency to be addressed separately. We also show that the terahertz pulses are found to be dispersionless and chirpless from the time-resolved experimental data. Here the steady state is defined as when the field is no longer amplified and is stable between round trips. This is typically on the nanosecond time scale. It should be noted that this is in contrast to frequency-comb operation, which takes orders-of-magnitude more round trips to fully stabilize. Nonetheless, the initial buildup dynamics of pulse generation can be explored where the large changes in the buildup occur over picosecond to nanosecond timescales. The theoretical model to simulate the buildup dynamics of the ultrashort pulses in mode-locked terahertz QCLs is compared with the experimental data, showing a good agreement, using the gain recovery time as a fitting parameter. By using the attainable parameters in the model, we find that femtosecond pulses are theoretically achievable in a terahertz QCL with gain recovery time on the scale of a few picoseconds if the gain bandwidth is over 1.6 THz and the associated allowable oscillating cavity modes could be increased dramatically. These findings deepen our understanding of the intricate mode-locking dynamics of semiconductor lasers and here in particular those of extreme class-*A* lasers, such as QCLs, where the gain recovery time is more than an order of magnitude smaller than the photon round-trip time.

II. SAMPLE

The QCL sample investigated here is based on a hybrid active region design that combines a bound-to-continuum and LO phonon depopulation scheme [39]. In this design, the $GaAs/Al_{0.15}Ga_{0.85}As$ material system is employed. The thicknesses of the quantum wells of the active region are 9.4, 11.5, 11.0, and 18.4 nm and those of the barriers are 4.2, 3.8, 1.8, and 5.5 nm. The 18.4-nm-thick quantum wells are doped at the level of 2.0×10^{16} cm^{-3}. The energy gap between the excited energy level and fundamental one is approximately 13.3 meV. This device is grown by molecular beam epitaxy followed by wafer bonding, and processed into 3-mm-long 100-μm-wide metal-metal waveguides [40,41]. A 3-mm cavity results in a photon round-trip time of approximately 80 ps. This

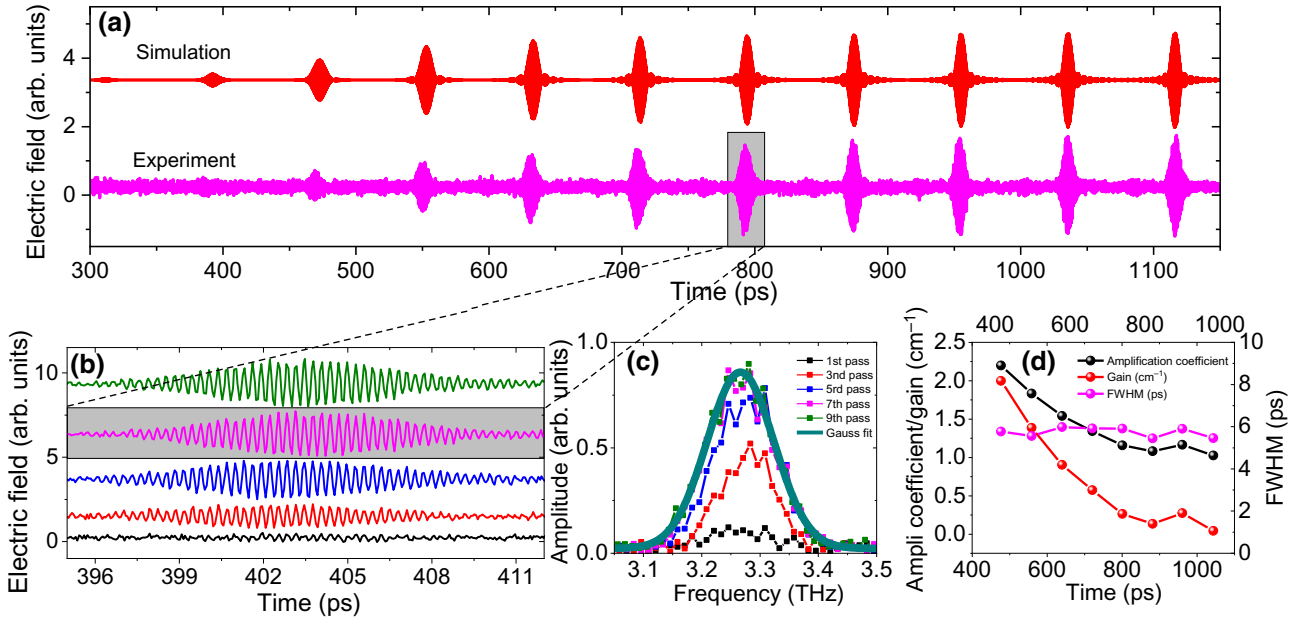

FIG. 3. Mode-locking switch-on dynamics of the terahertz QCL. (a) Phase-resolved emission of the mode-locked terahertz QCL in dynamics range. Bottom shows experiment; top shows simulations. (b) Enlargement of the $(2n+1)$th ($n=0$, 1, 2, 3, 4) terahertz pulses in (a) with clear view of the oscillation of phase-resolved electric field. (c) FFT spectra of the terahertz pulses in (b) from the first to ninth pass. Dark cyan curve denotes Gaussian fit of ninth pass spectrum. (d) FWHM (magenta), gain (red), and amplification coefficient (black) of the terahertz QCL as a function of time in mode-locked dynamic range.

hybrid depopulation scheme results in a spectral bandwidth lying between LO phonon and bound-to-continuum depopulation designs. The lasers operate at a center frequency of approximately 3.25 THz with emission spanning the range between 3.1 and 3.4 THz.

III. FREE-RUNNING SWITCH-ON DYNAMICS

The class of laser is the dominating factor regarding its transient behavior and how it is mode locked. In this section we investigate the free-running switch-on dynamics of a laser to determine the important parameters for the mode-locking buildup dynamics. For the lasing system, standard equations describe the evolution of the photon number (dF/dt) and population inversion ($d\Delta N/dt$) [42]. These equations are frequently used to characterize the steady-state emission by removing the time-dependent components (letting $dF/dt=0$ and $d\Delta N/dt=0$). However, its general solution towards steady state can be given by

$$F(t) = F_{\mathrm{ON}} + \delta F_{+} e^{\lambda_{+} t} + \delta F_{-} e^{\lambda_{-} t}, \tag{1}$$

$$\Delta N(t) = \Delta N_{\mathrm{ON}} + \delta N_{+} e^{\lambda_{+} t} + \delta N_{-} e^{\lambda_{-} t}, \tag{2}$$

where $F(t)$ and $\Delta N(t)$ are the time-dependent photon number and population inversion, F_{ON} and ΔN_{ON} are the photon number and population inversion at the steady state, and $\delta F_{\pm} e^{\lambda_{\pm} t}$ and $\delta N_{\pm} e^{\lambda_{\pm} t}$ are the transient components describing the dynamics of the laser towards its steady state. The laser behavior is governed by the exponents in Eqs. (1) and (2) and is given in the following:

$$\lambda_{\pm} = -\frac{r}{2\tau} \pm \frac{1}{2}\sqrt{\left(\frac{r}{\tau}\right)^2 - \frac{4(r-1)}{\tau\tau_{\mathrm{cav}}}}, \tag{3}$$

where $r=\Delta N_0/\Delta N_{\mathrm{th}}$ is the relative excitation (initial population inversion above lasing threshold), and τ and τ_{cav} are the excited electron lifetime and the lifetime of photons in the cavity, respectively. $\tau_{\mathrm{cav}} \gg \tau$ gives an exponential growth transient behavior (class-A laser), while $\tau_{\mathrm{cav}} < \tau$ or $\tau_{\mathrm{cav}} \sim \tau$ results in damped oscillation towards steady state (class B).

Figure 2(a) is the free-running emission of this QCL between 200 and 1800 ps, covering the full switch-on dynamics to the steady-state regime. Amplification can be observed from approximately 600 ps for around 300 ps, reaching a steady state at about 900 ps, as illustrated in Fig. 2(a). The emission is coherently detected using amplitude-and phase-resolved single-cycle terahertz pulses (of about 1 ps) and the experimental setup is detailed in Fig. 1.

From the phase-resolved emission data in Fig. 2(a), all the parameters (F_{ON}, $\delta F_{\pm}$, and $\lambda_{\pm}$) in Eq. (1) can be extracted, permitting full characterization of the lasing process. Here we are interested only in the switch-on dynamics, which are dominated by the parameter $\lambda_{\pm}$ in Eqs. (1) and (2). The black dots in Fig. 2(a) are chosen as the envelope of the QCL emission to represent the transient behavior from the amplification regime

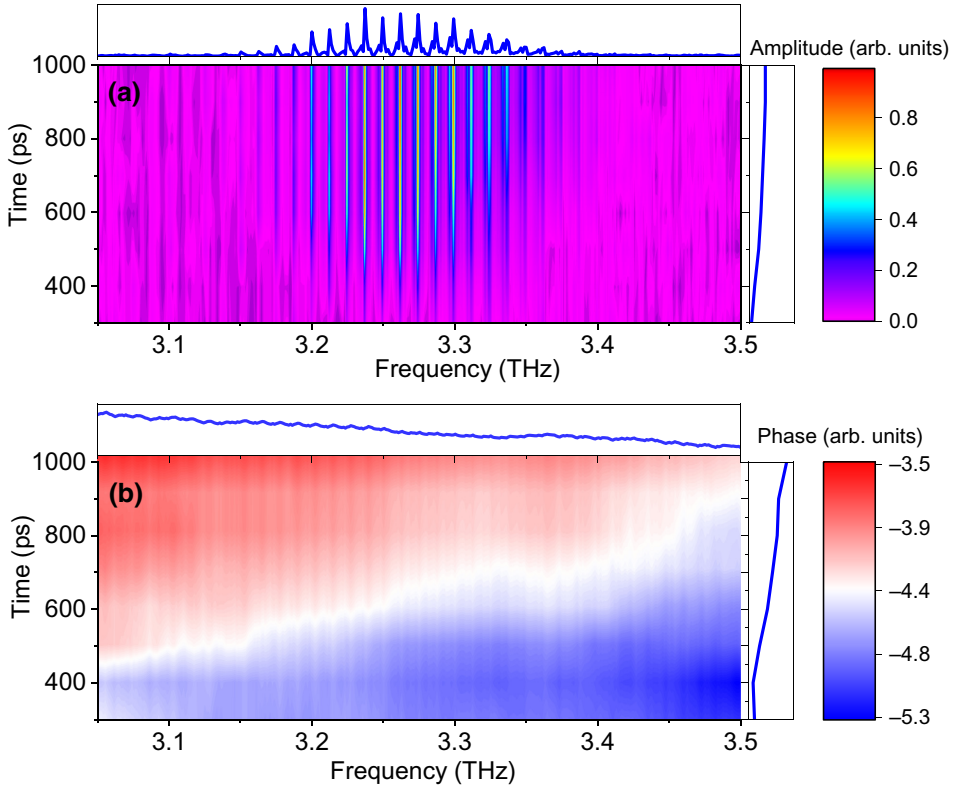

FIG. 4. Phase and amplitude dynamics of the terahertz QCL in mode-locking buildup regime. (a) The amplitude evolution of each longitudinal mode in the mode-locking buildup regime. Top, the spectral profile of (a) at 655 ps; right, the temporal profile at 3.286 THz. (b) The phase evaluation of each longitudinal mode in the mode-locking buildup regime. Top, the spectral profile of the figure at 655 ps; right, the temporal profile at 3.286 THz.

towards steady state. These dots are traced in Fig. 2(b) from the emission intensity (square of the amplitude). The exponential (nonoscillating) transient behavior shows typical class-A laser dynamics where $\tau_{\mathrm{cav}} \gg \tau$, leading to $\lambda_+ = -(r-1)/r\tau_{\mathrm{cav}}$, $\lambda_- = -r/\tau$, and $\lambda_- \gg \lambda_+$. The laser thus exponentially reaches its steady-state regime with an exponential time of $\tau_{\mathrm{relax}} = r\tau_{\mathrm{cav}}/(r-1) \approx \tau_{\mathrm{cav}}$. Therefore, the lifetime of the photon in the cavity can be experimentally estimated by fitting the transient emission of the QCL with an exponential function. For our QCL, a photon lifetime of the order of 100–200 ps in this double metal cavity is obtained as shown in Fig. 2(b). The photon lifetime in the laser cavity is a key parameter for characterizing a laser device, such as the losses per cavity round trip, the quality factor of the cavity, etc.

IV. MODE-LOCKING DYNAMICS

Active mode locking of terahertz QCLs can be achieved by applying a microwave modulation at or close to the round-trip frequency (i.e., around 12.25 GHz for this terahertz QCL) to modulate its gain across the entire gain medium. This permits the generation of a stable pulse train. In the following, we focus on the buildup dynamics of mode locking that has not been previously studied. Using the same injection seeding technique as for the free-running case, full-field-resolved emission of this mode-locked QCL in the dynamical regime is revealed in Fig. 3(a). The measurement is taken between 300 and 1100 ps. In this time window, the injected terahertz pulse propagates back and forth in the cavity and is simultaneously amplified. After about 880 ps, the gain is clamped to the losses and steady-state emission is achieved. Figure 3(a) also shows the simulated temporal profile of laser emission and is discussed in further detail in the following. Figure 3(b) shows an enlargement of the $(2n+1)$th ($n = 0$, 1, 2, 3, 4) terahertz pulses, shifted and offset to observe the same time window, where the terahertz frequency oscillations of the electric field can be clearly resolved. Interestingly, all pulses are in phase at every oscillation cycle and the duration (FWHM) is virtually unchanged during the whole dynamic range, as illustrated in Figs. 3(b) and 3(d). Figure 3(c) is the fast Fourier transform (FFT) of each light pulse of Fig. 3(b). This spectrum further confirms the broad emission frequency range spanning from 3.1 to 3.4 THz owing to the LO phonon depopulation scheme of the active region. The amplitude of the spectrum increases as the terahertz pulse propagates back and forth in the cavity,

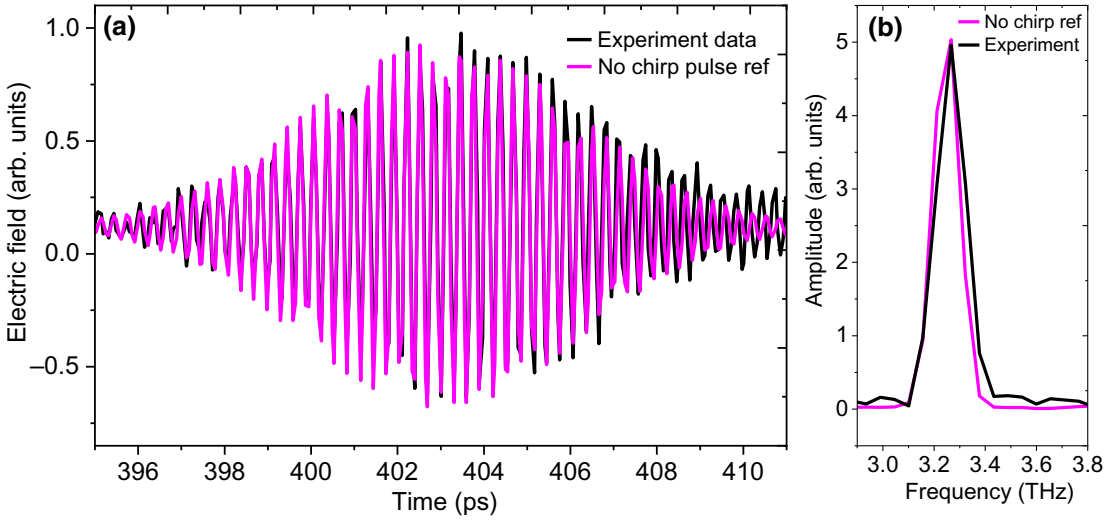

FIG. 5. Chirp analysis of the terahertz QCL. (a) The comparison of the ninth pass (black) and a chirpless terahertz pulse (magenta) with a carrier frequency of 3.24939 THz. (b) The spectra of the experimental data (black) and the chirpless pulse in (a).

and after a few round trips it is saturated, owing to the amplification of the terahertz pulses and gain clamping when laser action is initiated, respectively. The widths of the spectra are almost identical, further verifying that the amplification process in the mode-locking dynamic range has little influence on the pulse width (broadening or narrowing) in the time. The FFT spectrum fits well with a Gaussian-shaped function with the center located at 3.249 THz, equivalent to terahertz light pulses in the time domain also following a Gaussian distribution, as would be expected for mode-locked light pulses. The amplification coefficient (gain) in Fig. 3(d) (black(red)) defined as the ratio between sequential pulses in Fig. 3(a), starts at around 2.25 (2.0) cm^{-1} and then saturates at around 1 (0) cm^{-1} when steady state is achieved.

The field-resolved measurement in Fig. 3(a) not only permits us to obtain the total field or power evaluation of laser emission, but also provides an approach to gain detailed insights into the amplitude and phase transients of each longitudinal mode separately in the mode-locking buildup regime. As shown in Figs. 4(a) and 4(b), respectively, the amplitude and phase evaluation of each mode in the dynamical regime are extracted in both the frequency and time domain. The spectral profile of Fig. 4(a) at 655 ps is given at the top of the figure, which clearly shows the transient distribution of each mode. The quasi-Gaussian distribution of the spectrum further confirms the quasi-Gaussian distribution of the terahertz pulses in the time domain, as expected for mode-locked lasers. The temporal profile of Fig. 4(a) at 3.286 THz is given on the right-hand side of the main figure, from which the amplification process in this dynamical regime can be clearly observed. Similarly, the spectral and temporal profile of Fig. 4(b) are given at the top and right-hand side of the figure, respectively. Although detailed investigation of the phase transition is beyond the scope of the paper, it is important to notice that the phase is the most sensitive parameter of the electric field of laser emission. Any trivial physical process or environment change undergone by lasers can be reflected in the phase change. Therefore, our approach used in this paper permits us to reveal the underlying behaviors of a laser that cannot be easily obtained from amplitude change and permits realization of ultrasensitive QCL sensing in control experiments.

The full-electric-field-resolved mode-locking dynamics also permits direct access to the chirp dynamics of light pulses during the mode-locking buildup process. Figure 5(a) (black) shows one of the pulses (the ninth pass) in the saturated regime. The curve in magenta is a fit of the experimental data using a chirpless Gaussian pulse, $E(t) = E_0 \exp(-t^2/2\Delta t_0^2)e^{-i\omega_p t}$, where the carrier frequency $\omega_p/2\pi = 3.249\,39$ THz and the rms width $\Delta t_0 = 3.189\,29$ ps. From the beginning of the pulse at 394 ps until 407 ps, the experimental data match perfectly the chirpless Gaussian pulse form, especially in terms of oscillating frequency, indicating that the mode-locked terahertz pulse is chirpless. However, after 407 ps, the experimental pulse oscillates slightly faster than the carrier frequency ω_p. In addition, the amplitude of the experimental pulse is stronger than the calculated chirpless form. We attribute this anomaly to some high-frequency components mixing with the main pulse at the end of the falling edge where the temporal confinement from round-trip modulation is modest. The FFT of the experimental data and the chirpless Gaussian pulse further confirm the hypothesis, as shown in Fig. 5(b) where the two spectra are overlapped in the low-frequency regime, while the spectral amplitude of the experimental data is slightly stronger in the high-frequency regime.

TABLE I. Device parameters used in numerical simulations.

Symbol	Description	Value or definition
η_3	Injection efficiency into upper laser level (ULL)	54.41%
η_2	Injection efficiency into lower laser level (LLL)	1.65%
$I(t)$	Driving current of the laser cavity	$I(t) = I_0 + I_{\rm rf}\cos(\omega_{\rm rf}t)$
I_0	dc component of the driving current	0.75A
$I_{\rm rf}$	Modulation amplitude of the ac component of the current	0.15A
$\omega_{\rm rf}$	Modulation frequency of the driving current	$\omega_{\rm rf} = 2\pi\, \upsilon_{\rm RT}$
$\nu_{\rm RT}$	Laser cavity round trip frequency	12.25 GHz
G_m	Gain factor per period of mode m	$G_m = G_p/[1 + ((\nu_p - \nu_m)/(\Delta\nu/2))^2]/[1 + \varepsilon_{g,m}S_m(t)]$
G_p	Peak gain factor per period	133 s^{-1}
ν_m	Peak gain frequency	3.25 THz
$\Delta\nu$	FWHM of gain spectrum	300 GHz
$\beta_{\rm sp}$	Spontaneous emission factor	1.627×10^{-4}
τ_3	Total electron lifetime in ULL	5.5×10^{-12} s
τ_{32}	Nonradiative relaxation time from ULL to LLL	1.76×10^{-10} s
τ_2	Total electron lifetime in LLL	2.1×10^{-11} s
$\tau_{p,m}$	Photon lifetime for mode m	$\tau_{p,m} = 1/[\upsilon_{g,m}(\alpha_a + \alpha_m)]$
$\upsilon_{g,m}$	Group velocity of mode m	$\upsilon_{g,m} = c/n_{g,m}$
η_m	Power output coupling coefficient for mode m	Varies for modes
A	Small signal propagation loss	0.36
L_a	Laser cavity length	3 mm

V. MM RRE SIMULATION

In order to theoretically simulate the buildup dynamics of the ultrashort pulses in mode-locked terahertz QCLs and pulse propagation in the laser cavity, a self-consistent model is developed based on MM RREs [16–18] (see details in Supplemental Material [43]). By using the set of MM RREs, the amplitude and phase of each oscillating cavity mode can be simulated with the interaction effects of direct current modulation at the round-trip frequency, gain dependence on the mode frequency with saturation, and population inversion with ultrafast carrier lifetimes. The total electric field after mode competition and interference can then be obtained to study the formation of the optical field of pulses through active mode locking in terahertz QCLs. The mode number N_m is determined by the spectrum bandwidth, and is equal to 25 in this simulation to match the measured pulse spectrum. The parameters used in the equations are summarized in Table I. The envelope of the total pulse power from the longitudinal modes is calculated by

$$A(t) \propto \left| \sum_{m=1}^{N_m} \sqrt{P_m(t)}\, \exp[j\,(\omega_m t + \varphi_m(t))] \right|, \qquad (4)$$

where $P_m(t) = \eta_m \hbar \omega_m S_m(t)/\tau_{p,m}$ is the emission power in mode m; $\hbar$ is the reduced Planck constant; ω_m is the angular frequency of the mode m; S_m is photon population in eigenmode m. The gain compression factor for photon population of each longitudinal mode is adjusted to match the experimentally observed pulsed spectrum. When the MM RRE is solved over a continuous time scale of over ten round trips, both the pulse initialization and pulse propagation process in the laser cavity can be modeled, without assuming the initial pulse profile. The group-velocity dispersion of the gain medium can be described by the second-order dispersion β_2, which is calculated from the Kramers-Kronig relation, and its dependence on the frequency is shown in the Supplemental Material S3 [43]. The signal loss and pulse broadening due to gain dispersion can

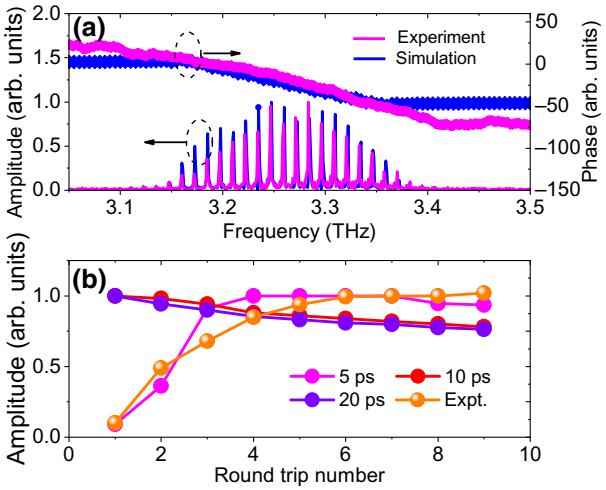

FIG. 6. Simulation of mode-locking buildup dynamics based on the MM RRE model. (a) The calculated (blue) and experimental (magenta) phase and amplitude in the frequency domain. (b) The pulse amplitude as a function of round-trip number for different electron lifetimes in the upper laser level and the comparison with the experimental result.

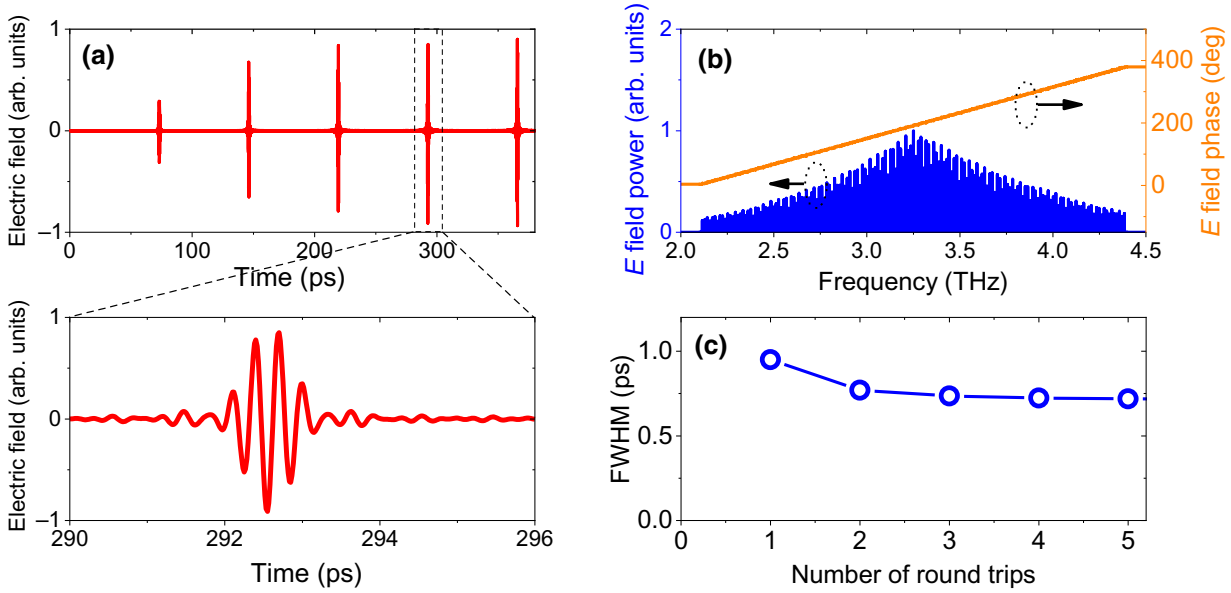

FIG. 7. Simulation of subpicosecond pulse (720 fs) with broad gain bandwidth (FWHM) of 1.6 THz. (a) The normalized electric field of the generated pulse in time domain; (b) the emission spectrum of the pulses (blue) and the electric field phase (orange) in frequency domain; (c) the pulse width (FWHM) as a function of the number of round trips.

be modeled in the frequency domain (through multiplication of the Fourier transform of the total electric field $A(t)$ by $\exp[(-\alpha + j\beta_2\omega^2)L_a]$ at the end of each laser cavity round trip). The balance between active current modulation and gain dispersion shapes the pulse profile of the terahertz QCL.

Based on the slowly varying envelope of the electric field, the relative phase between each longitudinal mode can be obtained, which allows us to get the electric field $E(t)$ of the laser emission in the time domain.

The transient evolution of the population inversion is driven by the injection current through active microwave modulation during the pulse buildup process. The phase and amplitude of each longitudinal mode are also obtained in the frequency domain from the simulations as shown in Fig. 6(a). This is in agreement with the experimental results. In this calculation, the upper lifetime of electrons is a critical parameter for the mode-locking buildup dynamics of QCLs and has an important impact on the time required to reach steady-state emission. As shown in the electric field in Fig. 3(a), an upper lifetime of around 5 ps gives a good fit with the experimental data, with the pulse amplitude increasing during the electric field buildup process and reaching steady state after 400 ps. Longer gain recovery times, despite still being shorter than the round-trip time, do not show this steady buildup of the pulses to reach the steady state as shown in Fig. 6(b). This clearly shows that the QCL is an extreme class-*A* laser with more than an order of magnitude difference between the round-trip and gain recovery times. The simulations also show that pulses are obtained instantly and do not need to reach the steady state to show this behavior, in agreement with the experiments. Furthermore, it is found that the smaller the value of the upper-level lifetime below 5 ps, the longer it takes for the pulse to be built up in the laser cavity. Importantly we find that such ultrafast gain on the few picosecond scale is not a hindrance to the realization of short pulses with a few picosecond duration from terahertz QCLs through active modulation. The gain bandwidth and associated allowable number of the oscillating cavity modes are the key limitations to achieving a subpicosecond duration pulse. As a theoretical example, Fig. 7 demonstrates a few cycle pulse with a duration of 720 fs from an actively mode-locked 3.2 THz QCL with the gain bandwidth of 1.6 THz and 167 longitudinal modes oscillating in the laser cavity if the gain dispersion can be compensated. Figures 7(a)–7(c) are the time-domain-normalized electric field, pulse spectrum (blue) with electric field phase spectrum (orange), and pulse width (FWHM) as a function of the number of round trips, respectively. This result shows that the femtosecond regime is achievable in a terahertz QCL with fast gain dynamics with the required gain bandwidth achievable through proven multistack active region and dispersion compensation designs.

To conclude, in this paper we bring together a theoretical and experimental investigation of the mode-locking buildup dynamics of a terahertz semiconductor laser. The dynamical process is phase- and amplitude-resolved on femtosecond timescales using an ultrafast coherent detection technique based on injection seeding. The experimental results are in good agreement with the theoretical calculation based on a theoretical model using MM RREs.

This model system uses QCLs and clearly shows a class-*A* laser with dynamics on the order of a few picoseconds, at least an order of magnitude shorter than the photon round-trip time. These advances will permit a predictive model for further advances in terahertz pulse generation from terahertz QCLs, realistically permitting subpicosecond pulse generation through broad gain structures and dispersion control for important applications such as gas metrology or terahertz nondestructive imaging. Further, the work marks a milestone in exploring and understanding the ultrafast mode-locking dynamics of semiconductor lasers in general, which will impact the dynamics of frequency-comb generation, ultrafast diagnostics, and mode-locking techniques. By the application of much shorter probe pulses, this theoretical and experimental approach can be applied to other laser systems in the midinfrared or even near-infrared to probe their ultrafast phase-resolved and mode-locked dynamics.

ACKNOWLEDGMENTS

This project has received funding from the European Union's Horizon 2020 research and innovation program under Grant No. 964735. The authors acknowledge funding from the French National Research Agency (Grant No. ANR-18-CE24-0013-02—"TERASEL"), Shenzhen Institute for Quantum Science and Engineering, Southern University of Science and Technology, Shenzhen International Quantum Academy, Australian Research Council Discovery Project (Grants No. DP160103910 and No. DP200101948) and EPSRC program "HyperTerahertz" (Grant No. EP/P021859/1). X.Q. acknowledges support under the Advance Queensland Industry Research Fellowships program. E.H.L. acknowledges support from the Royal Society and the Wolfson Foundation.

[1] G. Herink, B. Jalali, C. Ropers, and D. R. Solli, Resolving the build-up of femtosecond mode-locking with single-shot spectroscopy at 90 MHz frame rate, Nat. Photonics **10**, 321 (2016).

[2] P. Ryczkowski, M. Närhi, C. Billet, J.-M. Merolla, G. Genty, and J. M. Dudley, Real-time full-field characterization of transient dissipative soliton dynamics in a mode-locked laser, Nat. Photonics **12**, 221 (2018).

[3] U. Keller, Recent developments in compact ultrafast lasers, Nature **424**, 831 (2003).

[4] S. S. Dhillon, *et al.*, The 2017 terahertz science and technology roadmap, J. Phys. Appl. Phys. **50**, 043001 (2017).

[5] R. Kohler, Terahertz semiconductor-heterostructure laser, Nature **417**, 156 (2002).

[6] F. Wang, H. Nong, T. Fobbe, V. Pistore, S. Houver, S. Markmann, N. Jukam, M. Amanti, C. Sirtori, S. Moumdji, *et al.*, Short terahertz pulse generation from a dispersion compensated modelocked semiconductor laser, Laser Photonics Rev. **11**, 1700013 (2017).

[7] D. Bachmann, M. Rösch, M. J. Süess, M. Beck, K. Unterrainer, J. Darmo, J. Faist, and G. Scalari, Short pulse generation and mode control of broadband terahertz quantum cascade lasers, Optica **3**, 1087 (2016).

[8] J. Maysonnave, K. Maussang, J. R. Freeman, N. Jukam, J. Madéo, P. Cavalié, R. Rungsawang, S. P. Khanna, E. H. Linfield, A. G. Davies, H. E. Beere, D. A. Ritchie, *et al.*, Mode-locking of a terahertz laser by direct phase synchronization, Opt. Express **20**, 20855 (2012).

[9] D. Burghoff, T.-Y. Kao, N. Han, C. Wang, X. Cai, Y. Yang, D. J. Hayton, J.-R. Gao, J. L. Reno, and Q. Hu, Terahertz laser frequency combs, Nat. Photonics **8**, 462 (2014).

[10] F. P. Mezzapesa, K. Garrasi, J. Schmidt, L. Salemi, V. Pistore, L. Li, A. G. Davies, E. H. Linfield, M. Riesch, C. Jirauschek, *et al.*, Terahertz frequency combs exploiting an on-chip, solution-processed, graphene-quantum cascade laser coupled-cavity, ACS Photonics **7**, 3489 (2020).

[11] M. Rösch, G. Scalari, M. Beck, and J. Faist, Octave-spanning semiconductor laser, Nat. Photonics **9**, 42 (2014).

[12] L. Consolino, A. Taschin, P. Bartolini, S. Bartalini, P. Cancio, A. Tredicucci, H. E. Beere, D. A. Ritchie, R. Torre, M. S. Vitiello, and P. De Natale, Phase-locking to a free-space terahertz comb for metrological-grade terahertz lasers, Nat. Commun. **3**, 1040 (2012).

[13] M. Jaidl, N. Opačak, M. A. Kainz, S. Schönhuber, D. Theiner, B. Limbacher, M. Beiser, M. Giparakis, A. M. Andrews, G. Strasser, *et al.*, Comb operation in terahertz quantum cascade ring lasers, Optica **8**, 780 (2021).

[14] N. M. Burford and M. O. El-Shenawee, Review of terahertz photoconductive antenna technology, Opt. Eng. **56**, 010901 (2017).

[15] O. Schubert, M. Hohenleutner, F. Langer, B. Urbanek, C. Lange, U. Huttner, D. Golde, T. Meier, M. Kira, S. W. Koch, and R. Huber, Sub-cycle control of terahertz high-harmonic generation by dynamical Bloch oscillations, Nat. Photonics **8**, 119 (2014).

[16] X. Qi, I. Kundu, P. Dean, G. Agnew, T. Taimre, A. Valavanis, A. T. Grier, E. H. Linfield, A. G. Davies, D. Indjin, and A. D. Rakic, Mode selection and tuning mechanisms in coupled-cavity terahertz quantum cascade lasers, IEEE J. Sel. Top. Quantum Electron. **23**, 1 (2017).

[17] I. Kundu, F. Wang, X. Qi, H. Nong, P. Dean, J. R. Freeman, A. Valavanis, G. Agnew, A. T. Grier, T. Taimre, *et al.*, Ultrafast switch-on dynamics of frequency-tuneable semiconductor lasers, Nat. Commun. **9**, 3076 (2018).

[18] X. Qi, G. Agnew, T. Taimre, S. Han, Y. L. Lim, K. Bertling, A. Demić, P. Dean, D. Indjin, and A. D. Rakić, Laser feedback interferometry in multi-mode terahertz quantum cascade lasers, Opt. Express **28**, 14246 (2020).

[19] H. A. Haus, Mode-locking of lasers, IEEE J. Sel. Top. Quantum Electron. **6**, 1173 (2000).

[20] N. G. Usechak and G. P. Agrawal, Semi-analytic technique for analyzing mode-locked lasers, Opt. Express **13**, 2075 (2005).

[21] F. X. Kärtner, D. Kopf, and U. Keller, Solitary-pulse stabilization and shortening in actively mode-locked lasers, J. Opt. Soc. Am. B **12**, 486 (1995).

[22] D. Oustinov, N. Jukam, R. Rungsawang, J. Madéo, S. Barbieri, P. Filloux, C. Sirtori, X. Marcadet, J. Tignon, and S. Dhillon, Phase seeding of a terahertz quantum cascade laser, Nat. Commun. **1**, 1 (2010).

[23] J. Kröll, J. Darmo, S. S. Dhillon, X. Marcadet, M. Calligaro, C. Sirtori, and K. Unterrainer, Phase-resolved measurements of stimulated emission in a laser, Nature **449**, 698 (2007).

[24] B. S. Williams, Terahertz quantum-cascade lasers, Nat. Photonics **1**, 517 (2007).

[25] L. Li, L. Chen, J. Zhu, J. Freeman, P. Dean, A. Valavanis, A. G. Davies, and E. H. Linfield, Terahertz quantum cascade lasers with >1 W output powers, Electron. Lett. **50**, 309 (2014).

[26] S. Fathololoumi, E. Dupont, C. W. I. Chan, Z. R. Wasilewski, S. R. Laframboise, D. Ban, A. Mátyás, C. Jirauschek, Q. Hu, and H. C. Liu, Terahertz quantum cascade lasers operating up to 200 K with optimized oscillator strength and improved injection tunneling, Opt. Express **20**, 3866 (2012).

[27] L. Bosco, M. Franckié, G. Scalari, M. Beck, A. Wacker, and J. Faist, Thermoelectrically cooled THz quantum cascade laser operating up to 210 K, Appl. Phys. Lett. **115**, 010601 (2019).

[28] M. A. Kainz, M. P. Semtsiv, G. Tsianos, S. Kurlov, W. T. Masselink, S. Schönhuber, H. Detz, W. Schrenk, K. Unterrainer, G. Strasser, and A. M. Andrews, Thermoelectric-cooled terahertz quantum cascade lasers, Opt. Express **27**, 20688 (2019).

[29] A. Khalatpour, A. K. Paulsen, C. Deimert, Z. R. Wasilewski, and Q. Hu, High-power portable terahertz laser systems, Nat. Photonics **15**, 16 (2021).

[30] M. S. Vitiello, G. Scalari, B. Williams, and P. De Natale, Quantum cascade lasers: 20 years of challenges, Opt. Express **23**, 5167 (2015).

[31] S. Barbieri, M. Ravaro, P. Gellie, G. Santarelli, C. Manquest, C. Sirtori, S. P. Khanna, E. H. Linfield, and A. G. Davies, Coherent sampling of active mode-locked terahertz quantum cascade lasers and frequency synthesis, Nat. Photonics **5**, 306 (2011).

[32] F. Wang, V. Pistore, M. Riesch, H. Nong, P.-B. Vigneron, R. Colombelli, O. Parillaud, J. Mangeney, J. Tignon, C. Jirauschek, and S. S. Dhillon, Ultrafast response of harmonic modelocked THz lasers, Light: Sci. Appl. **9**, 51 (2020).

[33] J. R. Freeman, J. Maysonnave, H. E. Beere, D. A. Ritchie, J. Tignon, and S. S. Dhillon, Electric field sampling of modelocked pulses from a quantum cascade laser, Opt. Express **21**, 16162 (2013).

[34] F. Wang, K. Maussang, S. Moumdji, R. Colombelli, J. R. Freeman, I. Kundu, L. Li, E. H. Linfield, A. G. Davies, J. Mangeney, *et al.*, Generating ultrafast pulses of light from quantum cascade lasers, Optica **2**, 944 (2015).

[35] R. P. Green, A. Tredicucci, N. Q. Vinh, B. Murdin, C. Pidgeon, H. E. Beere, and D. A. Ritchie, Gain recovery dynamics of a terahertz quantum cascade laser, Phys. Rev. B **80**, 075303 (2009).

[36] D. R. Bacon, J. R. Freeman, R. A. Mohandas, L. Li, E. H. Linfield, A. G. Davies, and P. Dean, Gain recovery time in a terahertz quantum cascade laser, Appl. Phys. Lett. **108**, 081104 (2016).

[37] J. R. Freeman, J. Maysonnave, S. Khanna, E. H. Linfield, A. G. Davies, S. S. Dhillon, and J. Tignon, Laser-seeding dynamics with few-cycle pulses: Maxwell-Bloch finite-difference time-domain simulations of terahertz quantum cascade lasers, Phys. Rev. A **87**, 063817 (2013).

[38] J. Riepl, J. Raab, P. Abajyan, H. Nong, J. R. Freeman, L. H. Li, E. H. Linfield, A. G. Davies, A. Wacker, T. Albes, *et al.*, Field-resolved high-order sub-cycle nonlinearities in a terahertz semiconductor laser, Light: Sci. Appl. **10**, 246 (2021).

[39] M. I. Amanti, G. Scalari, R. Terazzi, M. Fischer, M. Beck, J. Faist, A. Rudra, P. Gallo, and E. Kapon, Bound-to-continuum terahertz quantum cascade laser with a single-quantum-well phonon extraction/injection stage, New J. Phys. **11**, 125022 (2009).

[40] S. Kumar, B. S. Williams, S. Kohen, Q. Hu, and J. L. Reno, Continuous-wave operation of terahertz quantum-cascade lasers above liquid-nitrogen temperature, Appl. Phys. Lett. **84**, 2494 (2004).

[41] Y. Chassagneux, J. Palomo, R. Colombelli, S. Barbieri, S. Dhillon, C. Sirtori, H. Beere, J. Alton, and D. Ritchie, Low threshold THz QC lasers with thin core regions, Electron. Lett. **43**, 41 (2007).

[42] *Light and Matter Ic / Licht Und Materie Ic, Encyclopedia of Physics/Handbuch Der Physik*, edited by L. Genzel (Springer, Berlin, Heidelberg, 1970), Vol. 5/25/2/2c.

[43] See Supplemental Material at http://link.aps.org/supplemental/10.1103/PhysRevApplied.18.064054 for further details of the model.